LMEC-69-11
General, Miscellaneous,
and Progress Reports

Corrosion of Type 18-18-2 Stainless Steel in 1200°F Static Sodium

By
W. T. Lee

LEGAL NOTICE

This report was prepared as an account of Government sponsored work. Neither the United States, nor the Commission, nor any person acting on behalf of the Commission:

A. Makes any warranty or representation, expressed or implied, with respect to the accuracy, completeness, or usefulness of the information contained in this report, or that the use of any information, apparatus, method, or process disclosed in this report may not infringe privately owned rights; or

B. Assumes any liabilities with respect to the use of, or for damages resulting from the use of any information, apparatus, method, or process disclosed in this report.

As used in the above, "person acting on behalf of the Commission" includes any employee or contractor of the Commission, or employee of such contractor, to the extent that such employee or contractor of the Commission, or employee of such contractor prepares, disseminates, or provides access to, any information pursuant to his employment or contract with the Commission, or his employment with such contractor.

Liquid Metal Engineering Center

Operated for
the U.S. Atomic Energy Commission by Atomics International
A Division of North American Rockwell Corporation

Contract: AT(04-3)-700

Issued: MAY 15 1969

This document is
PUBLICLY RELEASABLE
B Steele
Authorizing Official
Date: 5-23-06

DISTRIBUTION OF THIS DOCUMENT IS UNLIMITED
Pat

DISCLAIMER

This report was prepared as an account of work sponsored by an agency of the United States Government. Neither the United States Government nor any agency Thereof, nor any of their employees, makes any warranty, express or implied, or assumes any legal liability or responsibility for the accuracy, completeness, or usefulness of any information, apparatus, product, or process disclosed, or represents that its use would not infringe privately owned rights. Reference herein to any specific commercial product, process, or service by trade name, trademark, manufacturer, or otherwise does not necessarily constitute or imply its endorsement, recommendation, or favoring by the United States Government or any agency thereof. The views and opinions of authors expressed herein do not necessarily state or reflect those of the United States Government or any agency thereof.

DISCLAIMER

Portions of this document may be illegible in electronic image products. Images are produced from the best available original document.

ACKNOWLEDGMENT

The author wishes to acknowledge the guidance and suggestions of R. K. Wagner during preparation of this report. Many thanks are due to M. O. Malone and G. R. Prescott of C F Braun & Co for procuring the test materials. Appreciations is also extended to R. S. Kennedy, L. Cooper, and B. L. Claus for their contributions.

CONTENTS

	Page
Abstract	5
I. Introduction	7
II. Experiment	9
A. Test Materials	9
B. Testing	9
III. Results	13
A. Weight Gain Studies	13
B. Metallographic Studies	13
C. Electron Microprobe Studies	17
D. X-ray Diffraction Analysis	17
E. Tests on Type 304 SS Control Samples	17
IV. Discussion	25
A. Corrosion of Type 18-18-2 SS	25
B. Microstructural Changes	27
C. Silicon Depletion Process	27
D. Effect of Silicon Depletion	29
V. Conclusions	31
VI. Recommendations	33
References	35

TABLES

1. Chemical Composition of Type 18-18-2 SS and Type 304 SS	9
2. Corrosion Test Results of Type 18-18-2 SS and Type 304 SS in 1200°F Sodium (O_2 ~30 ppm)	13

FIGURES

Page

1. Microstructures of As-Received Type 18-18-2 SS and Type 304 SS. 10
2. Corrosion of Type 18-18-2 SS and Type 304 SS in 1200°F Sodium 12
3. Microstructures of Type 18-18-2 SS Exposed to 1200°F Sodium for Various Durations 14
4. Growth of Surface Reaction Zone of Type 18-18-2 SS and Type 304 SS in 1200°F Static Sodium (O_2 ~30 ppm) 16
5. Electron Microprobe Area Scans of Type 18-18-2 SS Exposed to 1200°F Static Sodium for 5060 hr. 18
6. Electron Microprobe Line Profiles of Type 18-18-2 SS Exposed to 1200°F Static Sodium for 5060 hr. 19
7. Growth of Silicon Depletion Zone in Type 18-18-2 SS in 1200°F Static Sodium. 20
8. Microstructure of Type 304 SS Exposed to 1200°F Sodium (O_2 ~30 ppm) for Various Durations 22
9. Electron Microprobe Area Scans of Type 304 SS Exposed to 1200°F Sodium for 5060 hr (800 magnification, 11-1/4 μ/ large division). 23
10. Electron Microprobe Line Profiles of Type 304 SS Exposed to 1200°F Sodium for 5060 hr (800 magnification, 11-1/4 μ/ large division). 24
11. Corrosion of Type 18-18-2 SS and Type 304 SS in 1200°F Sodium (in logarithmic form) 26
12. Silicon Depletion of Type 18-18-2 SS in 1200°F Sodium (O_2 ~30 ppm) 28
13. Effect of Silicon Additions on the Corrosion Resistance of 14 Cr - 14 Ni-Fe Alloys in HNO_3 plus Dichromate Solution 30

ABSTRACT

To determine the degree of corrosion or other degradation that Type 18-18-2 stainless steel (Cr-Ni-Si) would experience in a sodium environment, 18 coupons were immersed in 1200°F static sodium for periods up to 5060 hr. In addition, 12 Type 304 stainless steel tabs were simultaneously exposed for comparison. The average oxygen impurity in the sodium was about 30 ppm. The results of these preliminary tests show that Type 18-18-2 stainless steel is sufficiently corrosion-resistant in 1200°F sodium to warrant more thorough evaluation.

I. INTRODUCTION

Materials for use in sodium-heated, single-wall LMFBR steam generators will be subjected to stringent corrosive service environments. The material must be resistant to attack by liquid sodium as well as corrosion-resistant to water/steam. In addition, it must be strong enough to preclude leakage of water/steam into the sodium side for the entire design life (~30 yr) of the steam generator. Although ferritic steels (e. g., 2-1/4 Cr - 1 Mo) are stress corrosion-resistant to an aqueous/steam environment, their application in advanced sodium-heated steam generators is limited because of: (1) their low long-term mechanical properties at elevated temperatures (>1100°F), and (2) the potentially significant problem of decarburization and subsequent carburization of austenitic stainless steel in a sodium-cooled reactor system. While austenitic stainless steels exhibit adequate high-temperature strength and apparently experience no excessive mass transfer problem in sodium, they are not suitable for steam generator applications because of their high susceptibility to stress-corrosion cracking when exposed to an aqueous/steam environment containing minute amounts of chloride. Hence, there is an urgent need for new alloys that possess high-temperature strength, are compatible with liquid sodium, and are resistant to stress-corrosion cracking in an aqueous/steam environment.

Type 18-18-2 stainless steel (18 Cr - 18 Ni - 2 Si) is reported to display a remarkable resistance to stress-corrosion cracking and corrosion when exposed in an aqueous/ steam environment.[1] Tests also are reported to have shown that this high resistance to stress-corrosion cracking is attributed to the presence of an adequate amount of silicon in the steel, which increases the stability of the passive state of the alloy.[1,2] The higher nickel concentration (18 wt %) contributes only slightly to the stress-corrosion resistance of the steel.[3] In addition, Type 18-18-2 SS is reported to exhibit good weldability and to possess equivalent thermal properties when compared to other austenitic stainless steels.[1] This equivalence in thermal properties would be an added advantage due to the reduction in thermal stresses in the secondary reactor system. Therefore, an alloy with this high resistance to water/steam corrosion, coupled with high mechanical properties, would be attractive for steam generator applications. However, for service in a sodium-heated steam generator system,

the material must also be resistant to attack by sodium. To evaluate the degree of degradation Type 18-18-2 SS would experience in a sodium environment, preliminary corrosion tests were conducted in 1200°F static sodium for periods up to 5060 hr. In addition, twelve Type 304 SS tabs were simultaneously exposed for comparison purposes.

II. EXPERIMENT

A. TEST MATERIALS

The Type 18-18-2 SS test material (in sheet form, 0.1 in. thick) was produced by U. S. Steel Corporation. The compositions for Type 18-18-2 SS and for Type 304 SS are displayed in Table 1. The annealed and pickled Type 18-18-2 SS had a grain size of ASTM No. 3, and the annealed Type 304 SS had a grain size of ASTM No. 8.[4] Typical microstructures of Type 18-18-2 SS and Type 304 SS before testing are shown in Figure 1 (a and b, respectively).

TABLE 1

CHEMICAL COMPOSITIONS OF TYPE 18-18-2 SS AND TYPE 304 SS

Element	Type 18-18-2 SS (wt %)		Type 304 SS (wt %)
	Verification Analyses	Mill Report	Mill Report
Cr	20.71	18.30*	18.50
Ni	17.91	17.90*	10.70
Si	1.81	1.92*	0.61
Mn	1.47	1.51*	0.53
C	-	0.06	0.05
N	-	-	0.03
P	-	0.007	0.008
S	-	0.009	0.005
Mo	-	-	0.07
Al	-	-	0.005
Fe	Balance	Balance	Balance

*Obtained from A. W. Loginow, U. S. Steel Corp., Monroeville, Pa. for Heat No. 2P1227.

B. TESTING

After being sectioned into nominal size (1/2 in. by 1 in. by 0.1 in.), samples were measured individually for their dimensions and weight. Eighteen as-received Type 18-18-2 SS coupons were then immersed in 1200°F static

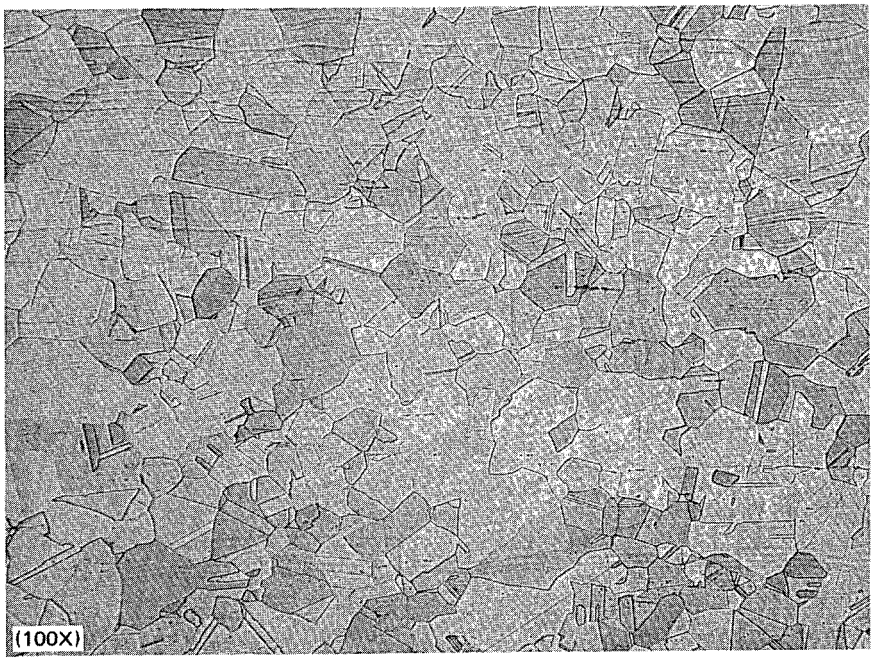

(a) AS-RECEIVED TYPE 18-18-2 SS

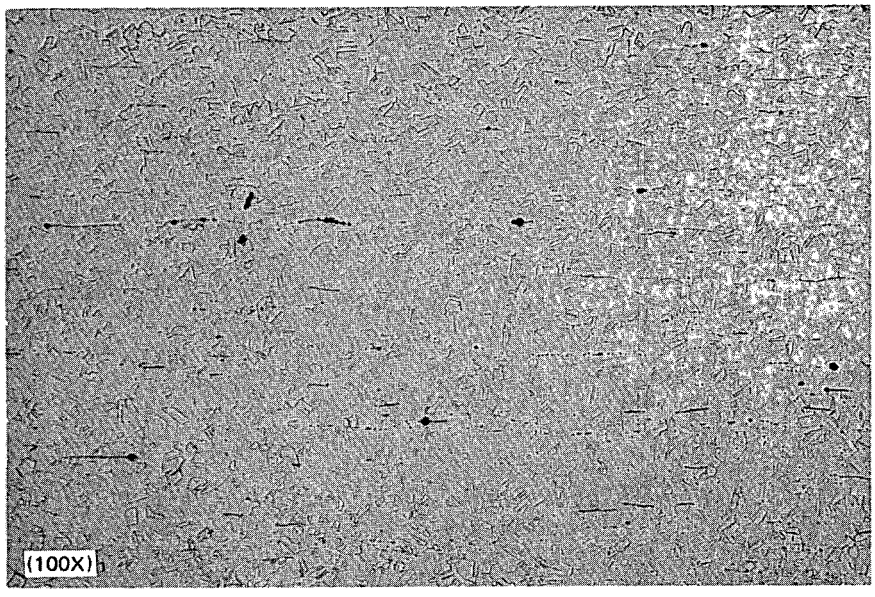

(b) AS-RECEIVED TYPE 304 SS

7693-4709

Figure 1. Microstructures of As-Received Type 18-18-2 SS and Type 304 SS (Etched with Marble's Reagent)

sodium (±5°F maximum) for exposures of 400, 1000, 3400, and 5060 hr. It should be noted, however, that the exposure time was not continuously isothermal at 1200°F for 400, 1000 hr, etc. Rather, they were the accumulative exposure times at 1200°F, since the sodium system had to be shut down about every 200 hr of operation for sample loading or unloading in conjunction with other experiments.

Twelve Type 304 SS tabs (1 in. by 1 in. by 0.03 in.) were also simultaneously exposed for comparison purposes. During test, average oxygen impurity in the sodium system was about 30 ppm.

After the samples were exposed for the required time in 1200°F sodium, the specimens were removed from the system and rinsed. Post-test dimensional and weight changes were recorded for each sample. Post-exposure examinations of the samples included electron microprobe analysis, metallography, and x-ray diffraction analysis.

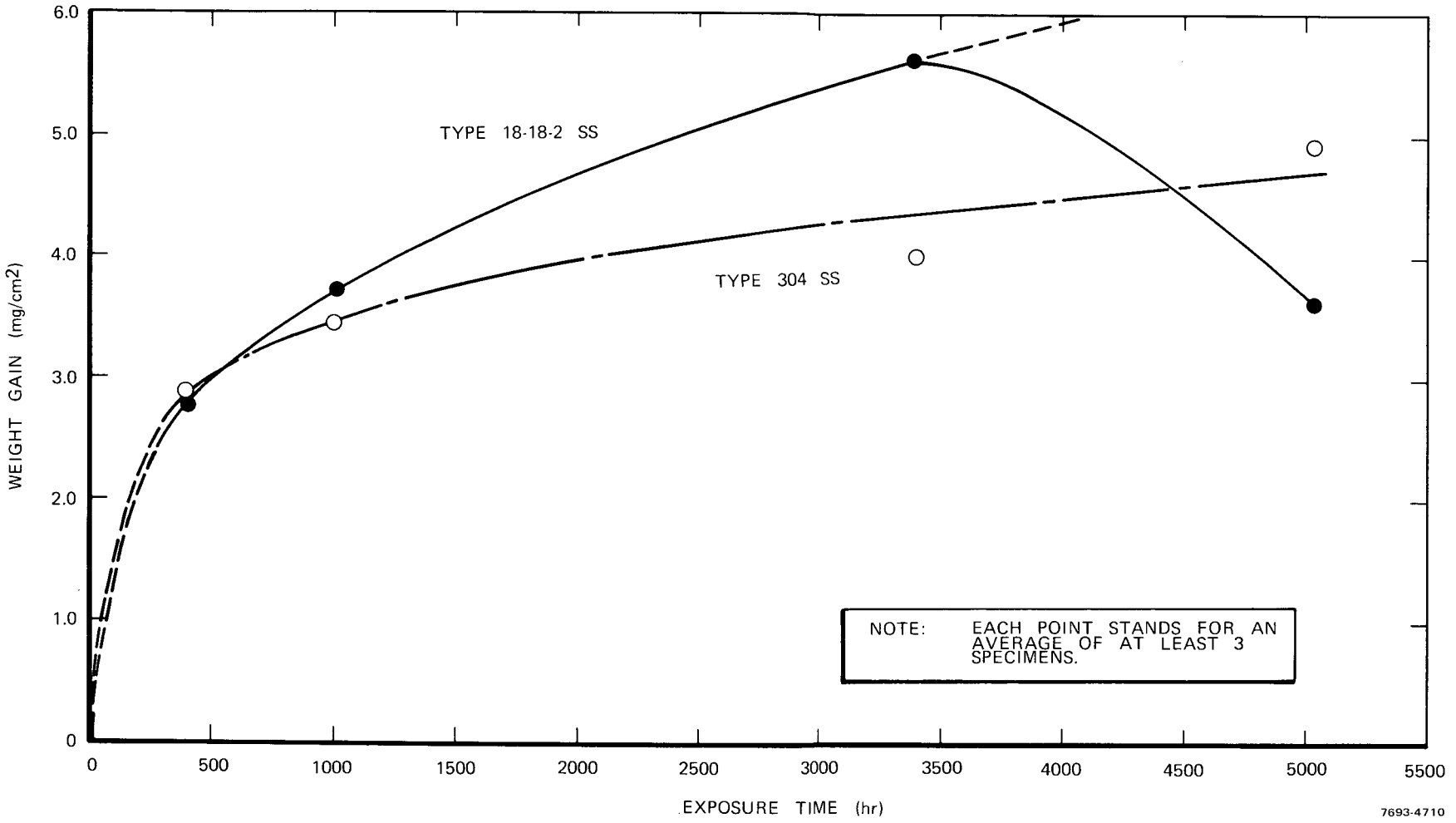

Figure 2. Corrosion of Type 18-18-2 SS and Type 304 SS in 1200°F Sodium

III. RESULTS

A. WEIGHT-GAIN STUDIES

Results of the corrosion test of Type 18-18-2 SS and Type 304 SS in 1200°F sodium (O_2 ~30 ppm) are shown in Table 2. Based on the weight-gain corrosion data developed, the corrosion rate of Type 18-18-2 SS was logarithmic up to 3400 hr of exposure in 1200°F sodium, as shown in Figure 2. The weight gain for 5060-hr samples, however, was significantly reduced when compared to that exposed to 3400-hr samples. As also shown in Figure 2, the corrosion rate of Type 18-18-2 SS is slightly higher than that of Type 304 SS.

TABLE 2

CORROSION RESULTS OF TYPE 18-18-2 SS AND TYPE 304 SS IN 1200°F SODIUM (O_2 ~30 ppm)

Exposure Time (hr)	Type 18-18-2 SS*				Type 304 SS*			
	Weight Gain (mg)	mg/cm^2	Reaction Layer (μ)	Post-Test Hardness	Weight Gain (mg)	mg/cm^2	Reaction Layer (μ)	Post-Test Hardness
400	23.40	2.79	18	R_a49 (R_b79)	36.70	2.87	0	R_a56 (R_b91)
1000	31.20	3.71	27	R_a53 (R_b86)	43.80	3.42	-	R_a70 (R_c39)
3400	45.50	5.61	45	R_a52 (R_b84)	51.20	4.00	30	R_a65 (R_c29)
5060	30.90	3.64	45	R_a51 (R_b83)	63.00	4.92	55	R_a64 (R_c27)

*An average value of at least three samples. Hardness of Type 18-18-2 SS before corrosion test = R_a44 (R_b70). Hardness of Type 304 SS before corrosion test = R_a50 (R_b81)

B. METALLOGRAPHIC STUDIES

Metallographic examination on the exposed Type 18-18-2 SS samples revealed a reaction zone (or depletion zone), as shown in Figure 3. The width of the reaction zone increased with exposure time, as displayed in Figure 4. Photomicrographs

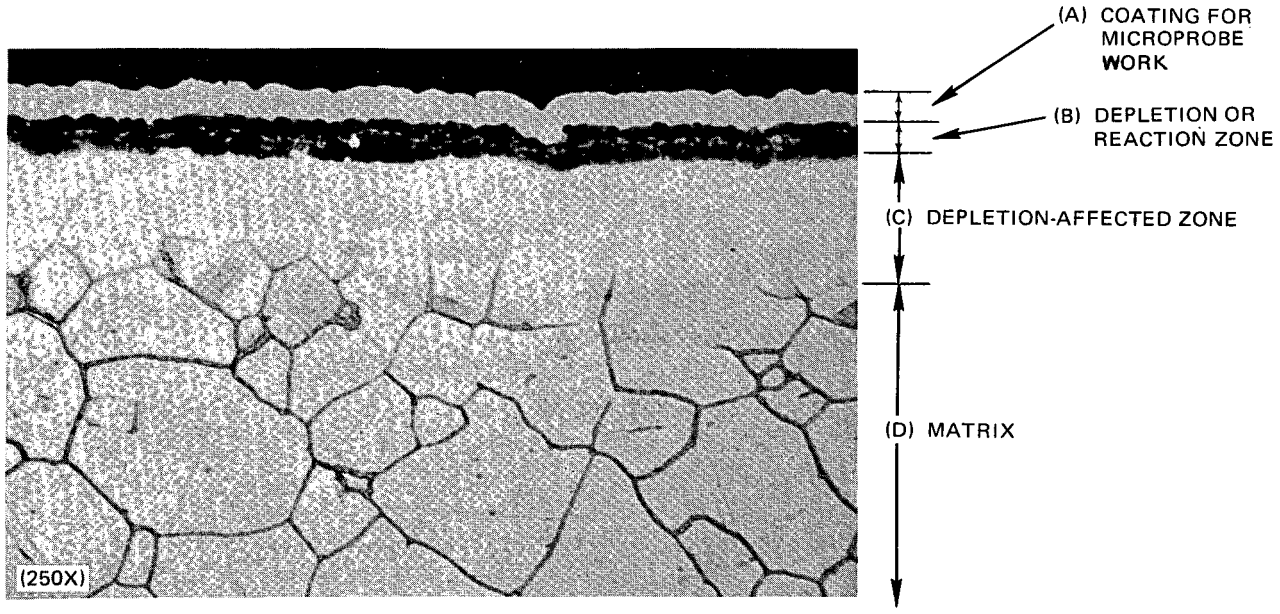

(a) EXPOSED FOR 400 hr

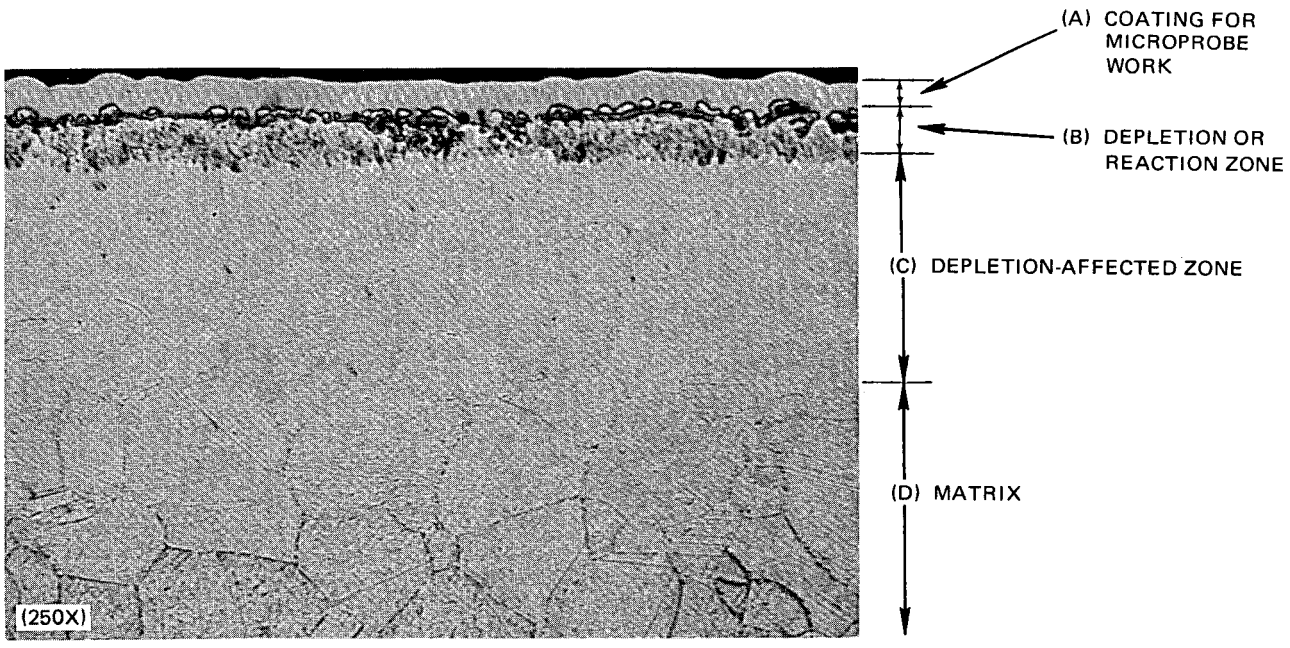

(b) EXPOSED FOR 1000 hr

7693-4711-1

Figure 3. Microstructures of Type 18-18-2 SS Exposed to 1200°F Sodium (O_2 ~30 ppm) for Various Durations (Etched with Marble's Reagent) (Sheet 1 of 2)

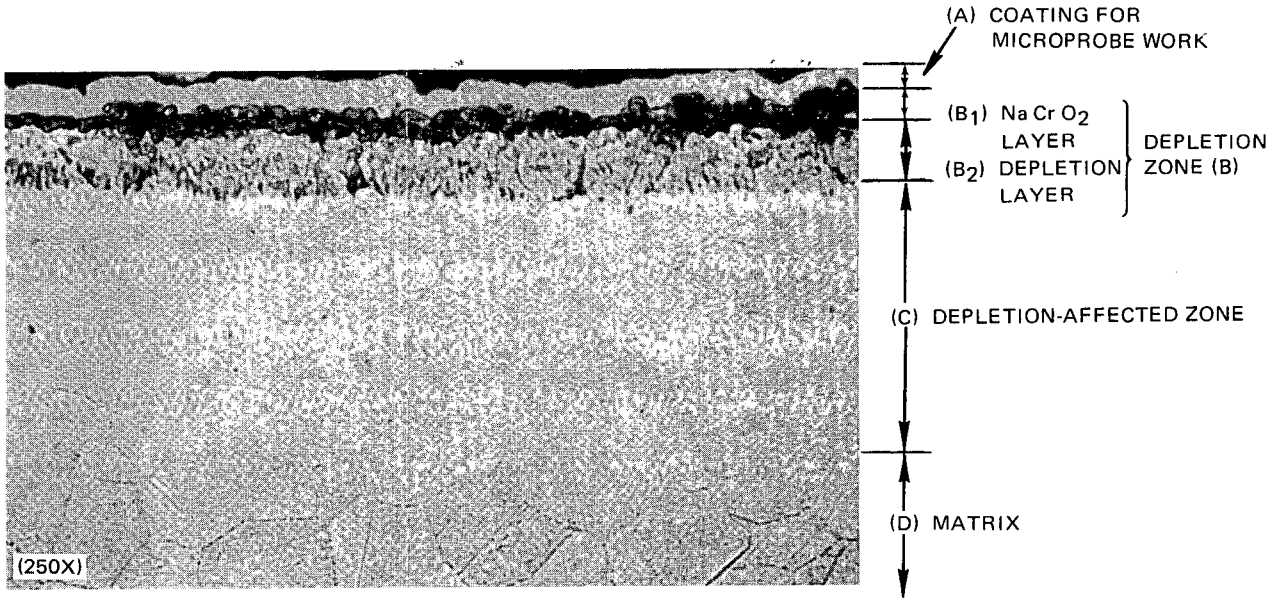

(c) EXPOSED FOR 3400 hr

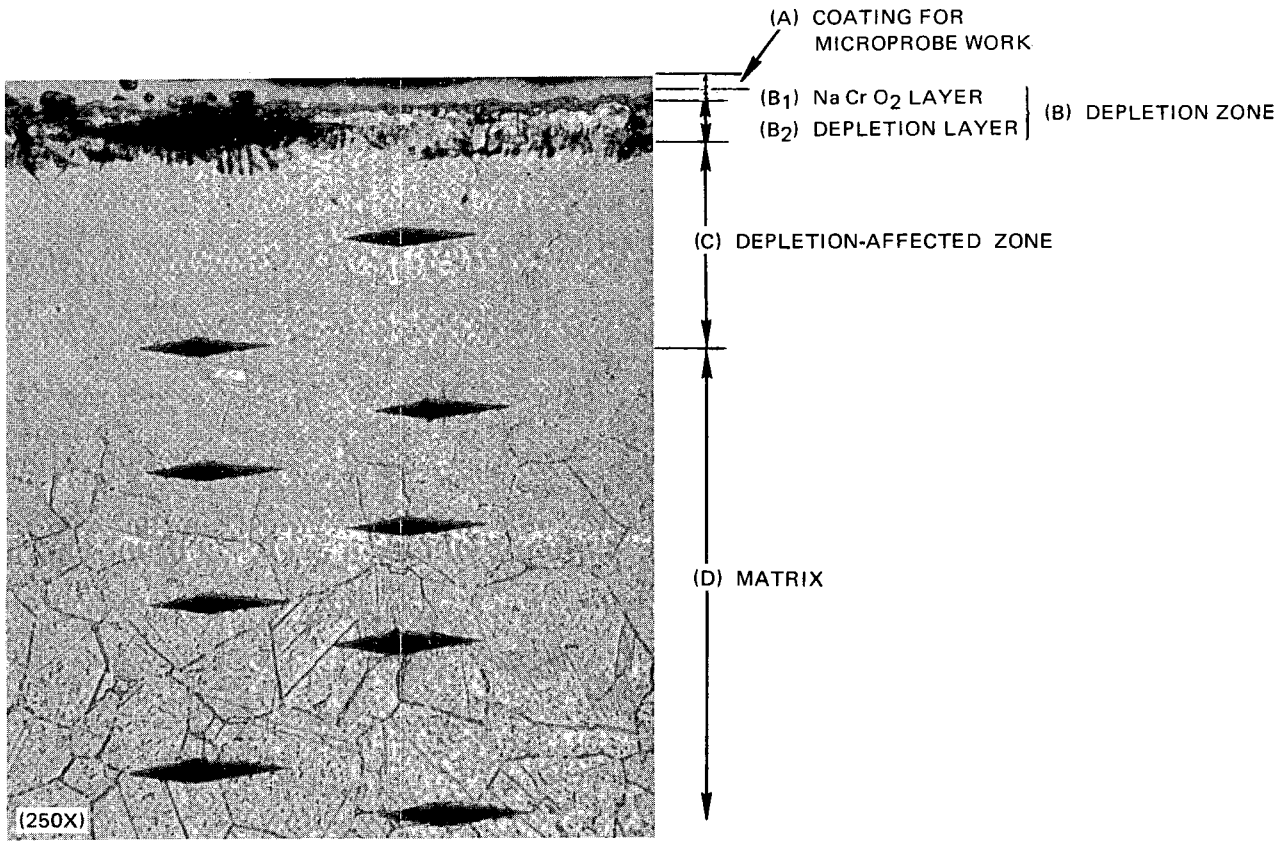

(d) EXPOSED FOR 5060 hr

7693-4711-2

Figure 3. Microstructures of Type 18-18-2 SS Exposed to 1200°F Sodium (O_2 ~30 ppm) for Various Durations (Etched with Marble's Reagent) (Sheet 2 of 2)

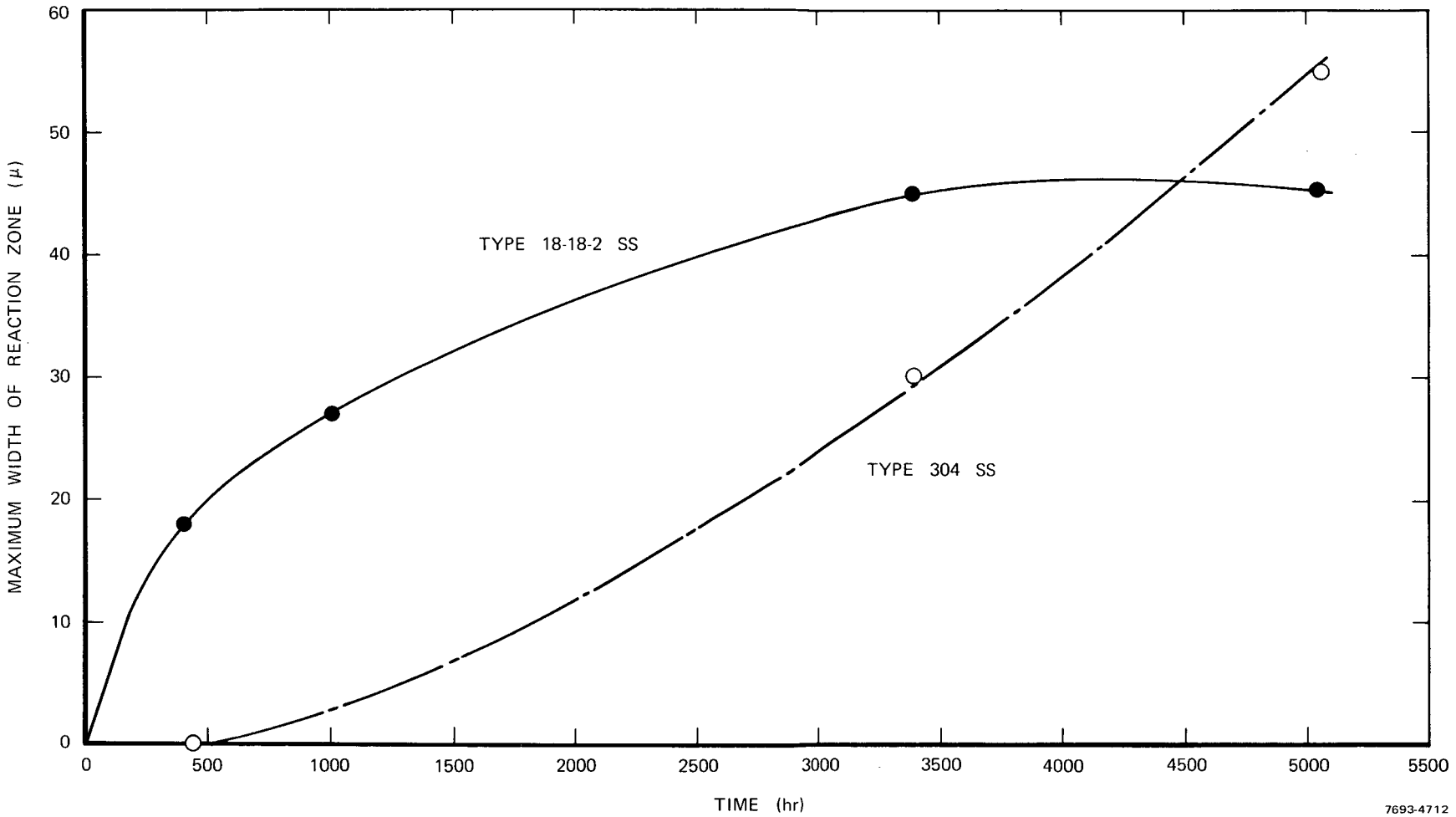

Figure 4. Growth of Surface Reaction Zone of Types 18-18-2 and 304 SS in 1200°F Na (O_2 ~30 ppm)

of Type 18-18-2 SS samples (Figure 3) also showed a second zone next to the first depletion zone, where the grain boundaries were diffused, and carbide precipitates were relatively absent. In addition, the grains in the zone exhibited a lighter contrast when compared to the microstructures in the unaffected matrix (see Figure 3d). It is noteworthy that the width of this second zone increased with time up to 3400 hr. But the 5060-hr samples exhibited a narrower second zone when compared to that found in 3400-hr samples. Also shown in Figure 3 is a small amount of discontinuous carbide precipitation in grain boundaries, twin boundaries, and in the grain matrix. A second-phase material was found in the depletion zone. Some oxides were also found in the inner junction of the depletion zone. Post-test hardness of all Type 18-18-2 SS samples was found to be slightly increased (from $R_b 70$ to $R_b 82$).

C. ELECTRON MICROPROBE STUDIES

Electron microprobe area scans and line profiles of a 5060-hr sample are shown in Figures 5 and 6, respectively. The results revealed two principal reaction layers — a chromium-rich outer layer, and an iron/nickel-rich, chromium depleted layer. The silicon content in the reaction zone was depleted. The silicon depletion was logarithmic with time up to 5060 hr, as shown in Table 2 and Figure 7. For the 5060-hr sample, the silicon appeared to be completely depleted in a reaction zone 0.002 in. deep, as shown in Figure 6. Manganese was also depleted from this zone.

D. X-RAY DIFFRACTION ANALYSIS

X-ray diffraction analysis of the surface film on Type 18-18-2 SS exposed to 1200°F sodium for 5060 hr revealed a green layer of amorphous film with some crystalline $NaMO_2$ oxide, where M is predominantly chromium with lesser amounts of Fe and Ni. With the surface oxide layer removed, x-ray diffraction of the surfaces of the 3400-hr and 5060-hr samples revealed ferrite in the second layer of the reaction zone. X-ray scan on the matrix revealed only trace amounts of $M_{23}C_6$ carbide precipitates. No sigma phase was found.

E. TESTS ON TYPE 304 SS CONTROL SAMPLES

Metallographic examination of Type 304 SS samples also revealed a surface sodium chromite oxide layer (as identified by x-ray diffraction) which increased

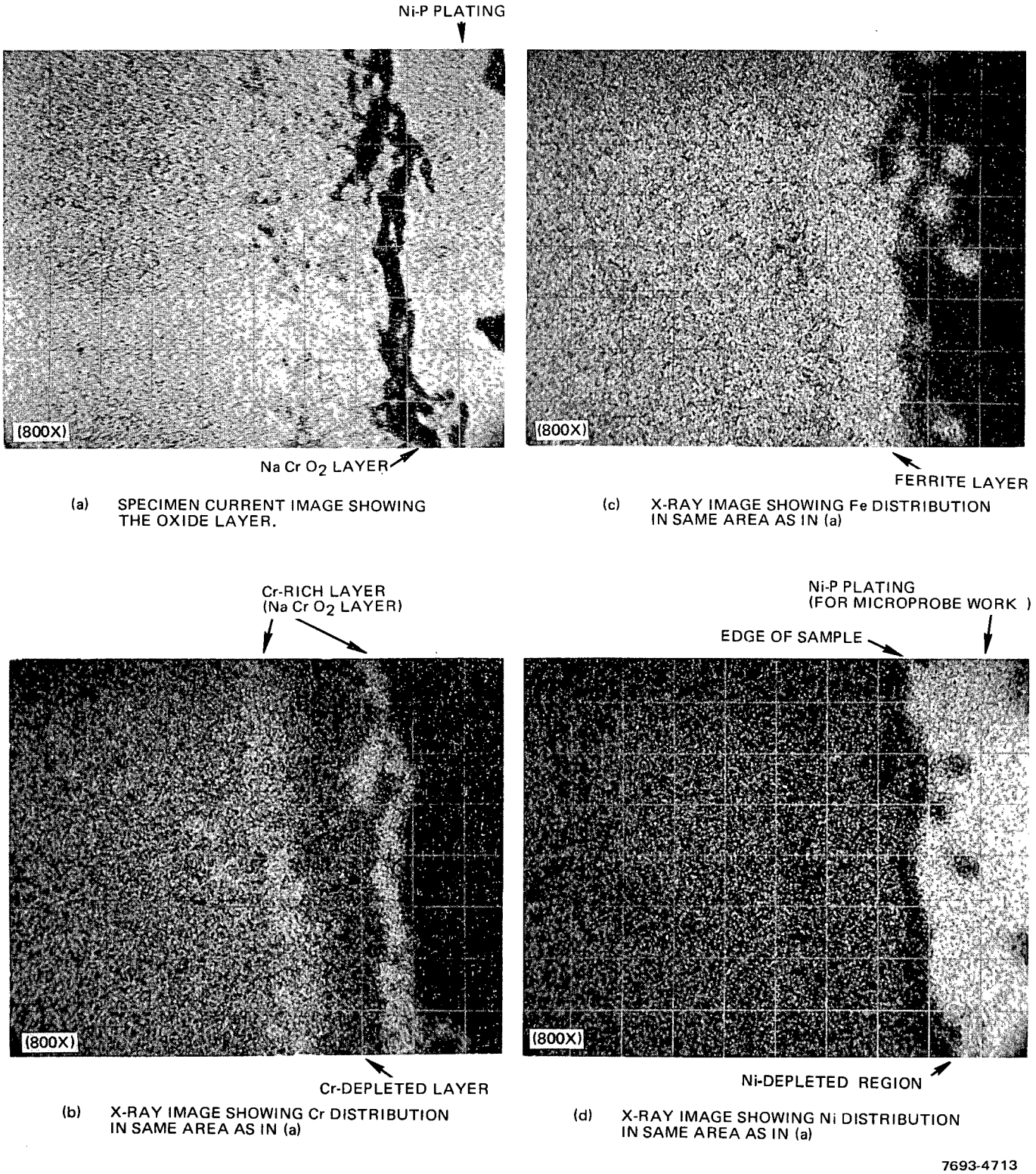

Figure 5. Electron Microprobe Area Scans of Type 18-18-2 SS Exposed to 1200°F Sodium ($O_2 \sim 30$ ppm) for 5060 hr (11-1/4 μ/large division)

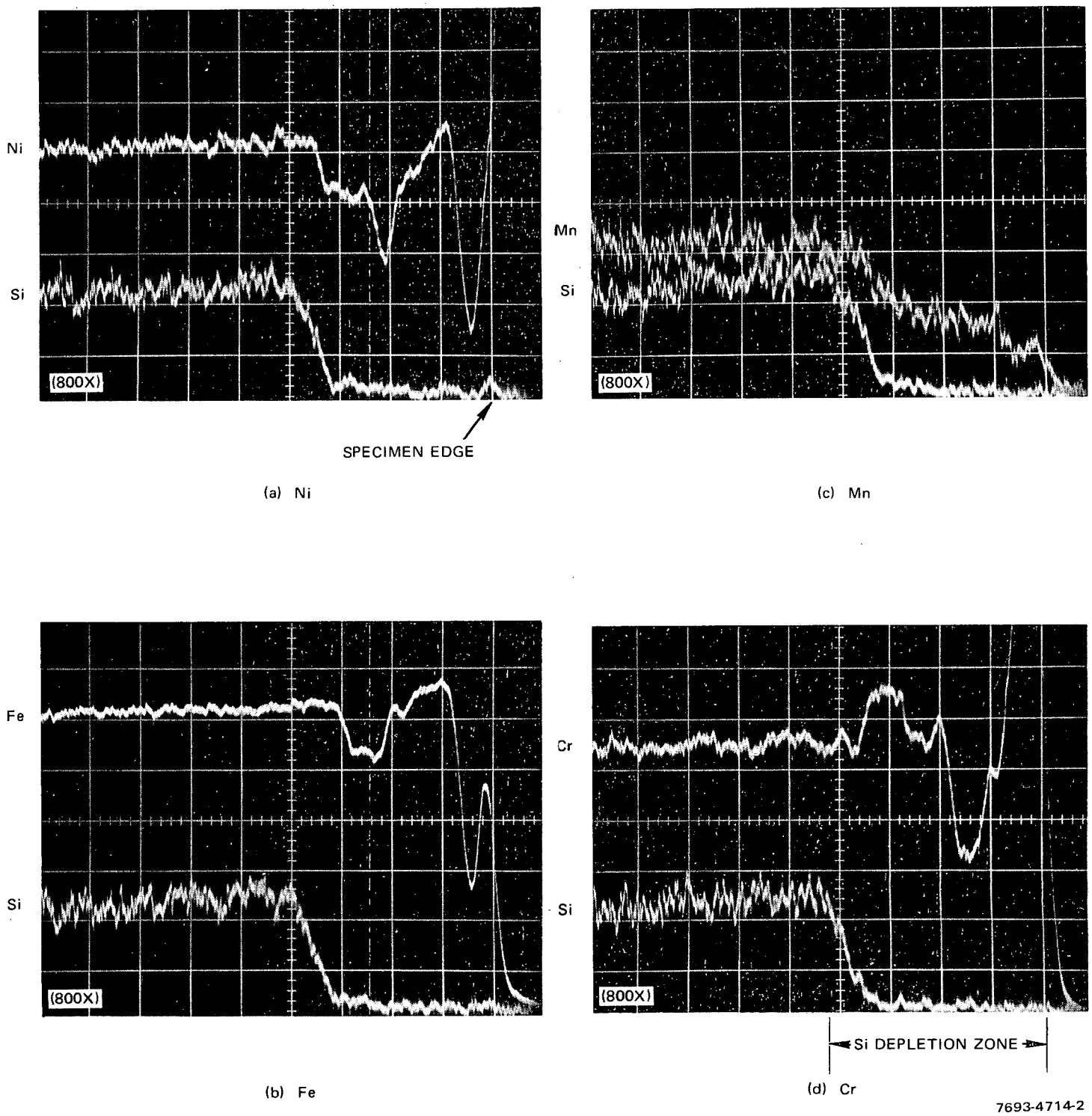

Figure 6. Electron Microprobe Line Profiles of Type 18-18-2 SS Exposed to 1200°F Sodium (O_2 ~30 ppm) for 5060 hr (11-1/4 μ/large division)

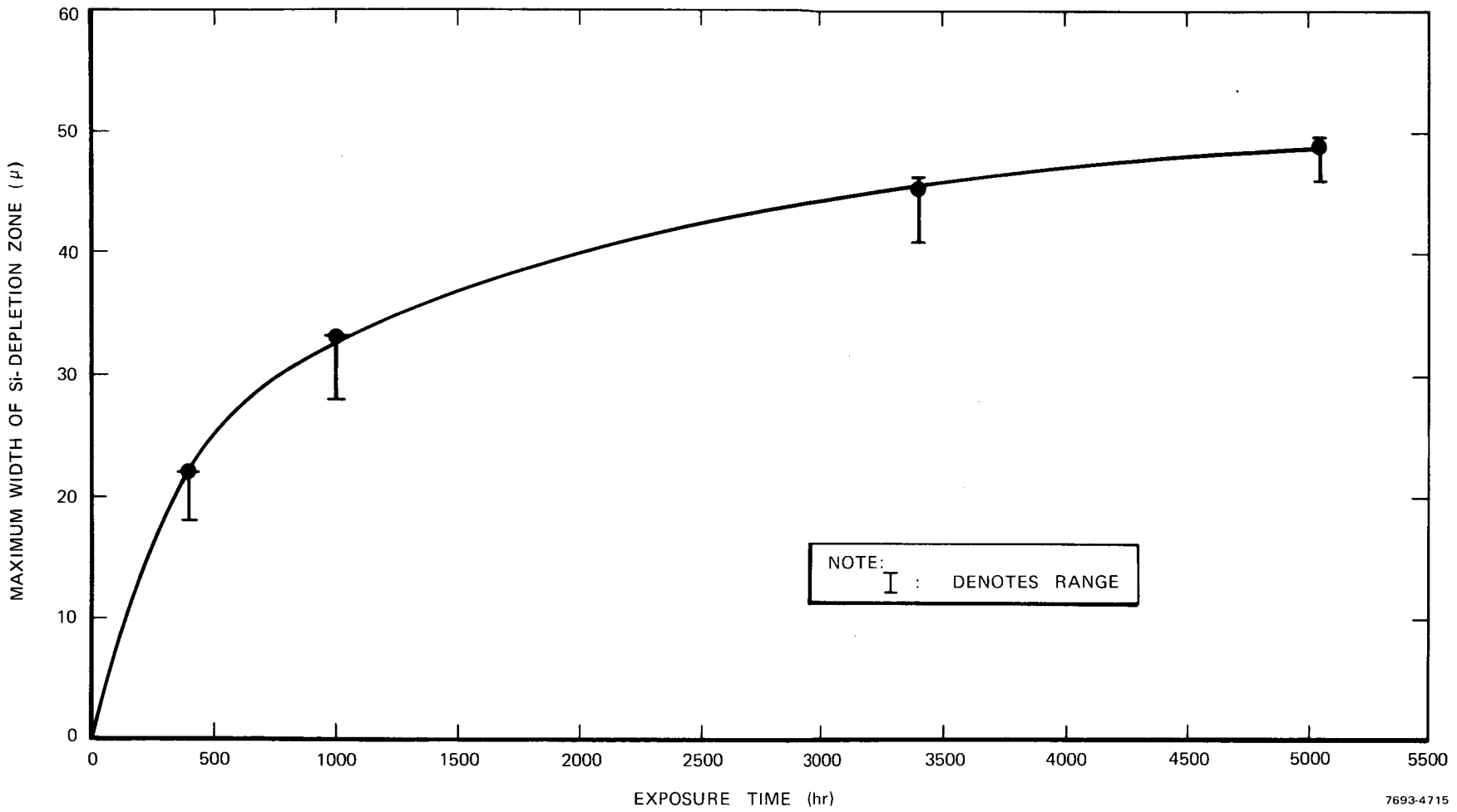

Figure 7. Growth of Silicon Depletion Zone in Type 18-18-2 SS in 1200°F Static Sodium ($O_2 \sim 30$ ppm)

with exposure time. Normal carbide precipitation on grain boundaries and twin boundaries were observed. However, it should be noted that the oxide layer, found adherent to the matrix, appeared to have penetrated into the sample matrix along grain boundaries (Figure 8). This ingress of sodium chromite into the sample can be seen in the electron microprobe specimen current image photos (Figure 9a and b). Electron microprobe data also indicated that the outer surface oxide layer was high in Cr and followed by a thin layer of high Fe/Ni, Cr-depleted ferrite layer, as shown in Figure 10a, b, and d. The post-test hardness of all specimens was increased significantly (from R_b81 to R_c31).

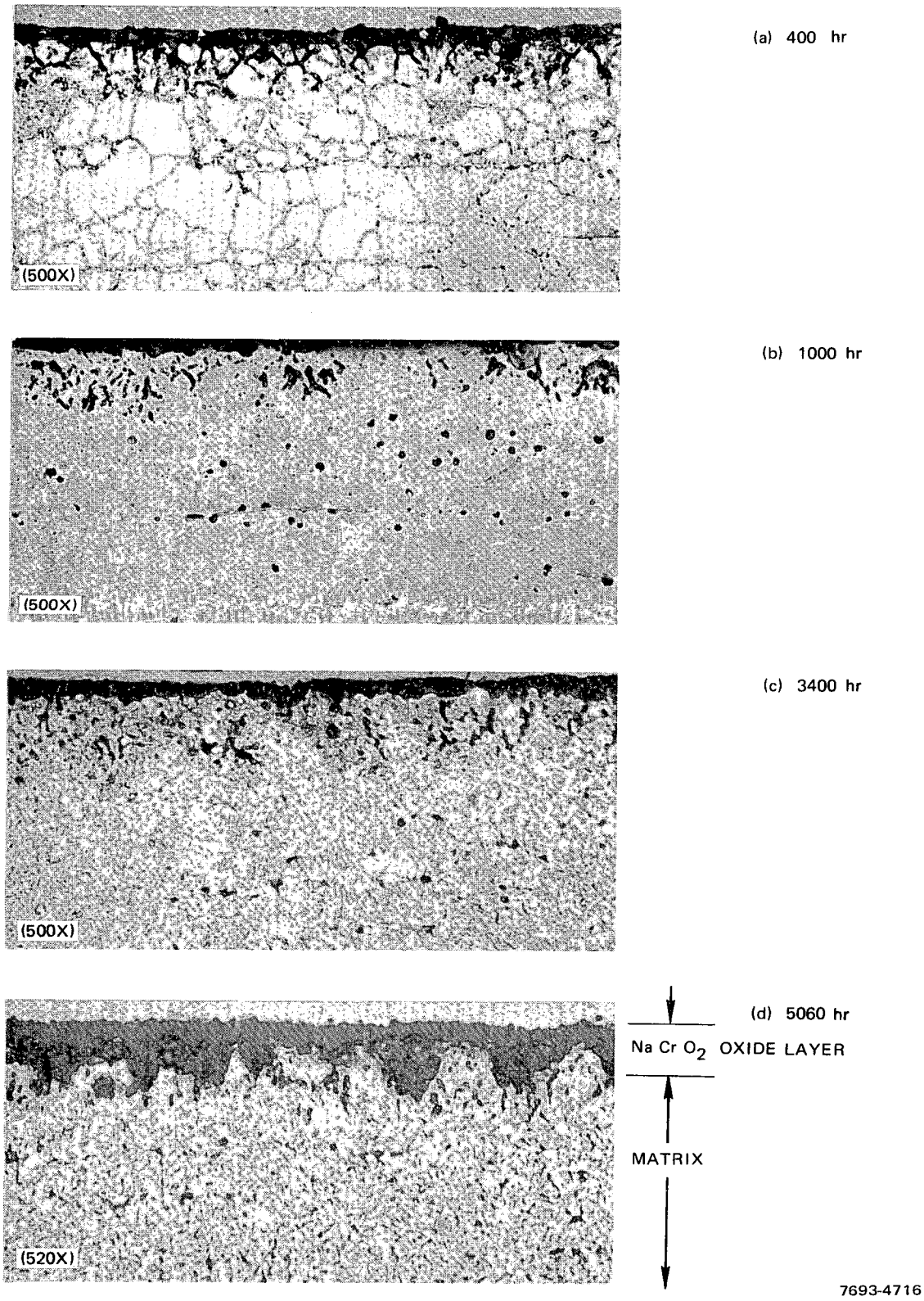

Figure 8. Microstructure of Type 304 SS Exposed to 1200°F Sodium (O_2 ~30 ppm) for Various Durations (Etched with Marble's Reagent)

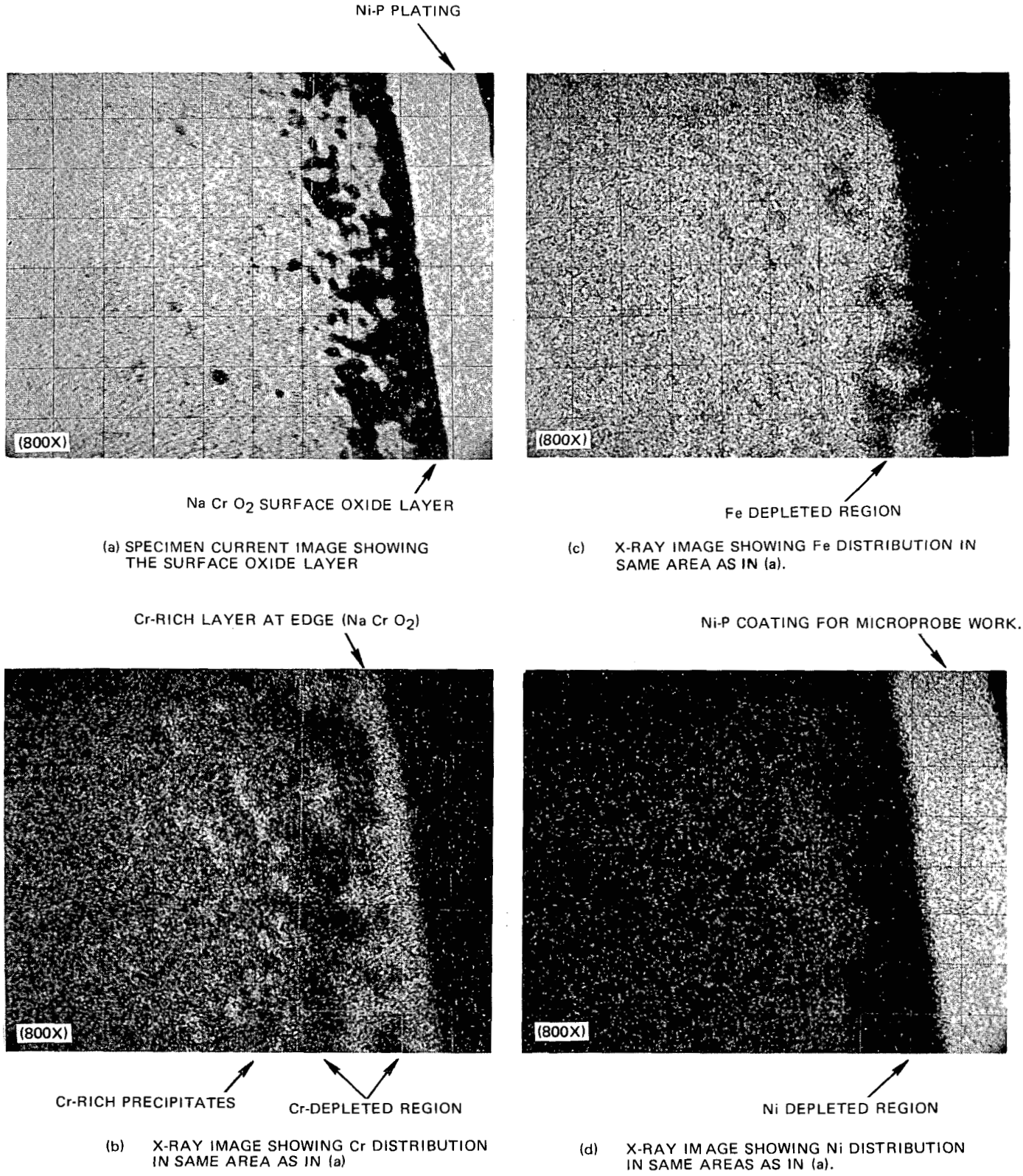

Figure 9. Electron Microprobe Area Scans of Type 304 SS Exposed to 1200°F Sodium (O_2 ~30 ppm) for 5060 hr (11-1/4 μ/large division)

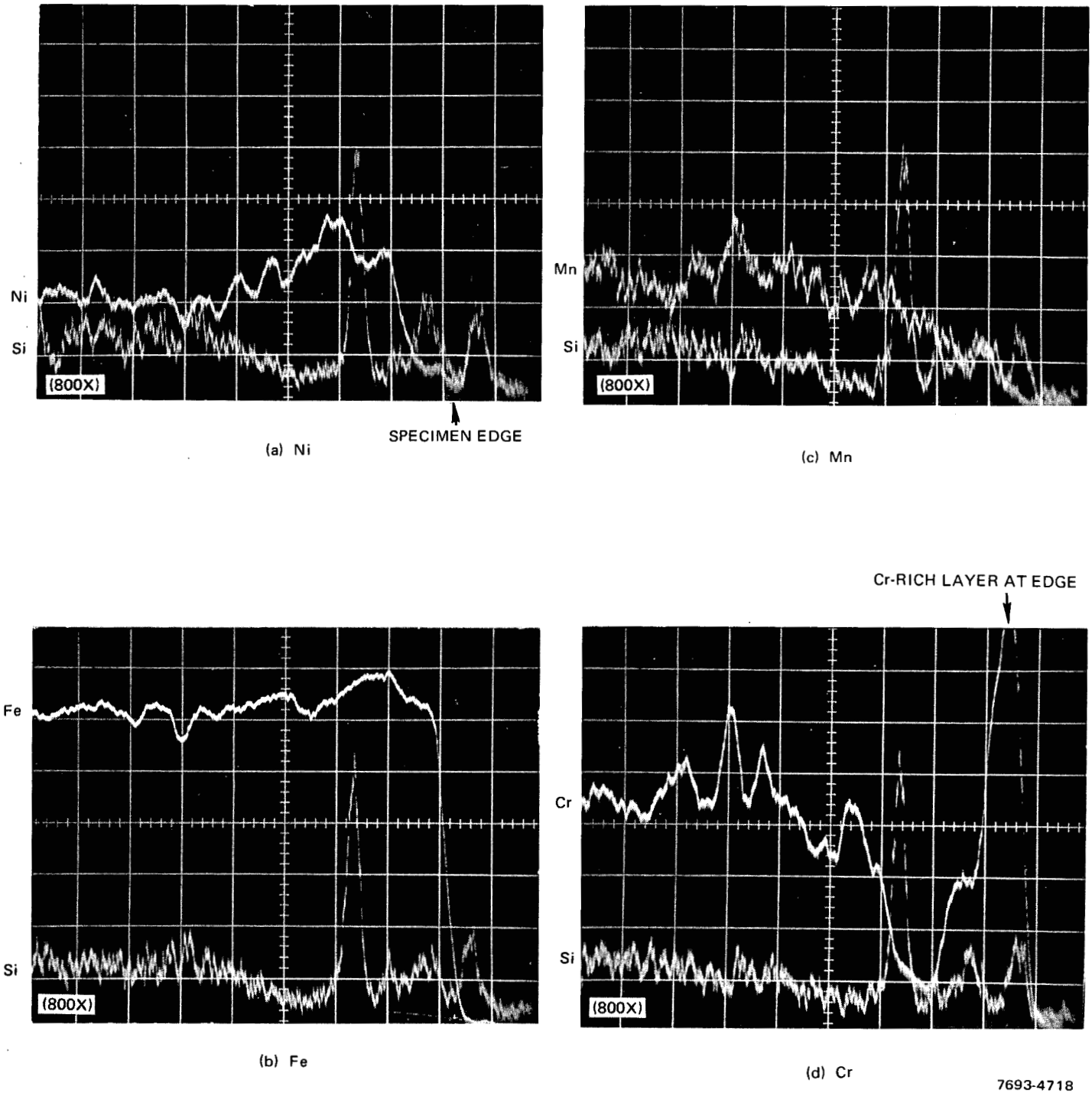

Figure 10. Electron Microprobe Line Profiles of Type 304 SS Exposed to 1200°F Sodium (O_2 ~30 ppm) for 5060 hr (11-1/4 μ/large division)

IV. DISCUSSION

A. CORROSION OF TYPE 18-18-2 SS

Based on the weight gain corrosion data shown in Figure 11, the corrosion rate of Type 18-18-2 SS was logarithmic up to 3400 hr of exposure in 1200°F sodium(O_2 ~30ppm). The weight gain for 5060-hr samples, however, was significantly reduced when compared to that exposed to 3400-hr samples. The reduction in weight gain beyond 3400 hr was caused by the breakdown of non-adherent surface oxide film at the outer surface of the reaction zone. Electron microprobe and metallographic results further substantiated this exfoliation of surface oxide film on Type 18-18-2 SS samples. The breakaway of surface oxide film was attributed to the presence of silicon in the alloy. Similar breakdown of surface oxide film due to the presence of silicon was also reported in other silicon alloys.[5,6,7] The development of nonadherent surface oxide film could be further enhanced by the thermal cycling mode of operation adopted for the sodium system (70 to 1200°F and 1200 to 70°F) because of the thermal stresses generated in the surface oxide layer.

It is noteworthy that the adherency of surface oxide film on Type 304 SS samples was good, and it was not adversely affected by thermal cycling, at least up to 5060 hr of exposure. The surface oxide film found on Type 18-18-2 SS and Type 304 SS was formed by oxygen impurity in sodium. While the presence of oxide in the reaction zone of Type 18-18-2 SS increased the post-test hardness in the depletion zone, hardness increase in the matrix was attributed to precipitation hardening caused by thermal aging.

Comparison of the corrosion rates of Type 18-18-2 SS and Type 304 SS in 1200°F sodium indicated that Type 18-18-2 SS exhibited a higher corrosion rate. More specifically, the corrosion rates of Type 18-18-2 SS and Type 304 SS are 7.2 $mg/cm^2/yr$ (~1.2 mil/yr), and 5.2 $mg/cm^2/yr$ (~1 mil/yr), respectively, based on the extrapolated corrosion data (Figure 11). The higher corrosion rate of Type 18-18-2 SS was attributed to the formation of nonadherent surface oxide scale and the wider ferrite layer in the depletion zone. Loss of this protective film could accelerate corrosion due to the exposure of new surfaces for attack.[7] In addition, the higher diffusion rate in the ferrite lattice could have further enhanced the corrosion rate of Type 18-18-2 SS.

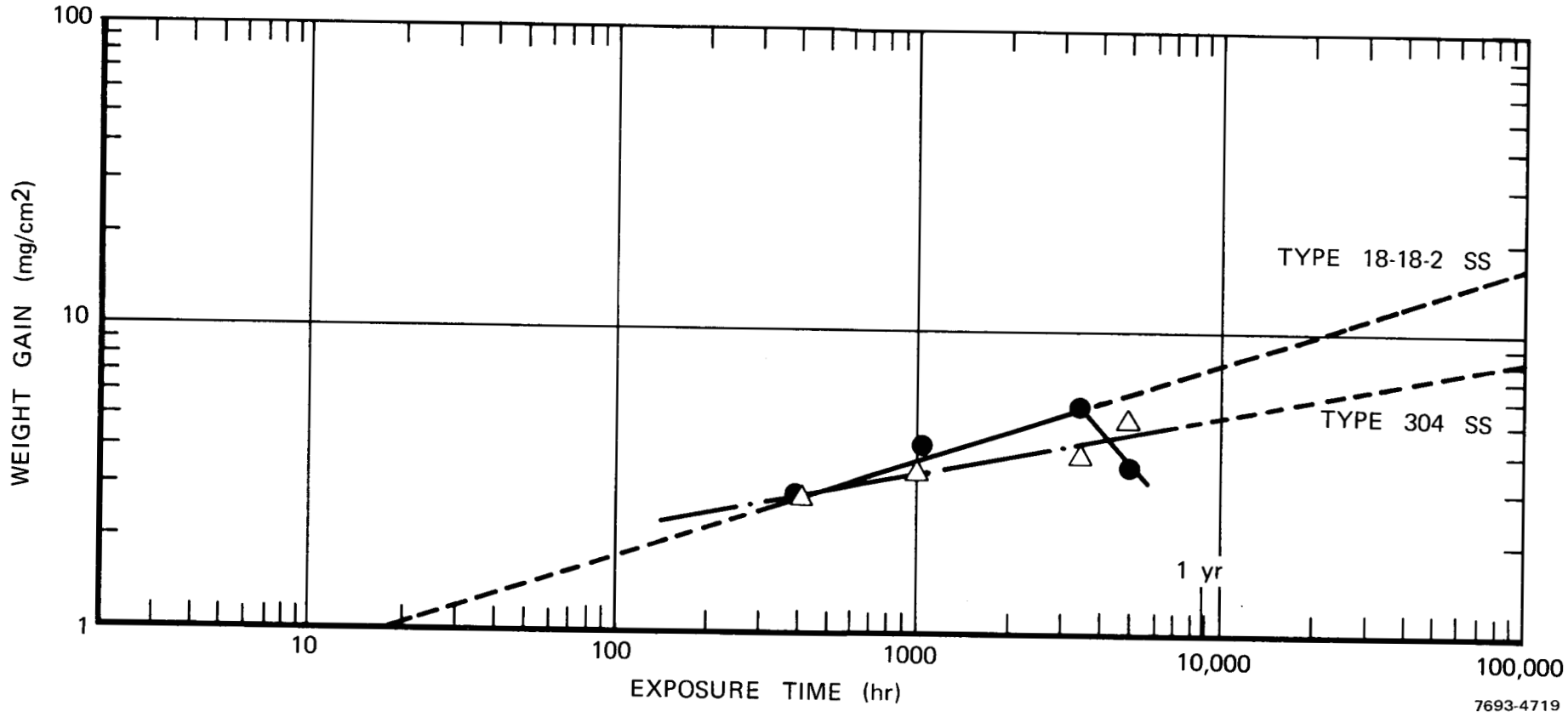

Figure 11. Corrosion of Type 18-18-2 SS and Type 304 SS in 1200°F Sodium ($O_2 \sim 30$ ppm)

B. MICROSTRUCTURAL CHANGES

Formation of a ferrite layer in a static sodium environment appeared to be an "anomalous" corrosion behavior. The development of a ferrite layer on the surface of austenitic stainless steel samples is usually associated with selective leaching of Cr and Ni in a dynamic sodium system, where thermal-gradient and concentration-gradient mass-transfer conditions are operative. However, in this experiment, the samples were immersed in an "isothermal static" system with periodic replenishment of sodium (where mass transfer could take place by a dissolution process due to the presence of a concentration gradient). The sodium environment acted as a constant sink for chromium, nickel, silicon, and manganese. In addition, the formation of $NaCrO_2$ at the sample surfaces depleted chromium in the vicinity close to the oxide layer, as found by electron microprobe analysis (Figure 5b). Therefore, it can be concluded that the selective depletion of chromium and/or nickel and the formation of $NaCrO_2$ led to an α-iron-rich region in the depletion zone.

It is interesting to note that some oxides were also found in the inner junction of the reaction zone, as shown in Figures 3 and 5. Electron microprobe results confirmed a high-chromium layer at the inner junction between the reaction zone and the metal matrix (Figure 5b). These observations suggest that the high-oxygen sodium might have migrated into the inner surface of the depletion zone, thus forming oxide at the junction. "Intergranular penetration" of high oxygen sodium into sample matrix was also observed in Type 304 SS samples, as shown in Figure 8c and d where the grain morphology was drastically changed. This grain boundary oxide formation, coupled with normal carbide precipitation, contributed to a significant increase in the post-test hardness values of all exposed Type 304 SS specimens (see Table 2). This ingress of sodium along grain boundaries was not generally found in austenitic stainless steels exposed to high-purity 1200°F static sodium ($\sim$10 ppm O_2) for 4000 hr.[8] Inpurities in sodium (metallic and nonmetallic, e.g., O_2, C, etc.) could conceivably have caused the ingress of sodium along grain boundaries where crystal imperfections are high.

C. SILICON DEPLETION PROCESS

The kinetics of silicon depletion of Type 18-18-2 SS in 1200°F sodium is logarithmic, as displayed in Figure 12. The silicon depletion process is

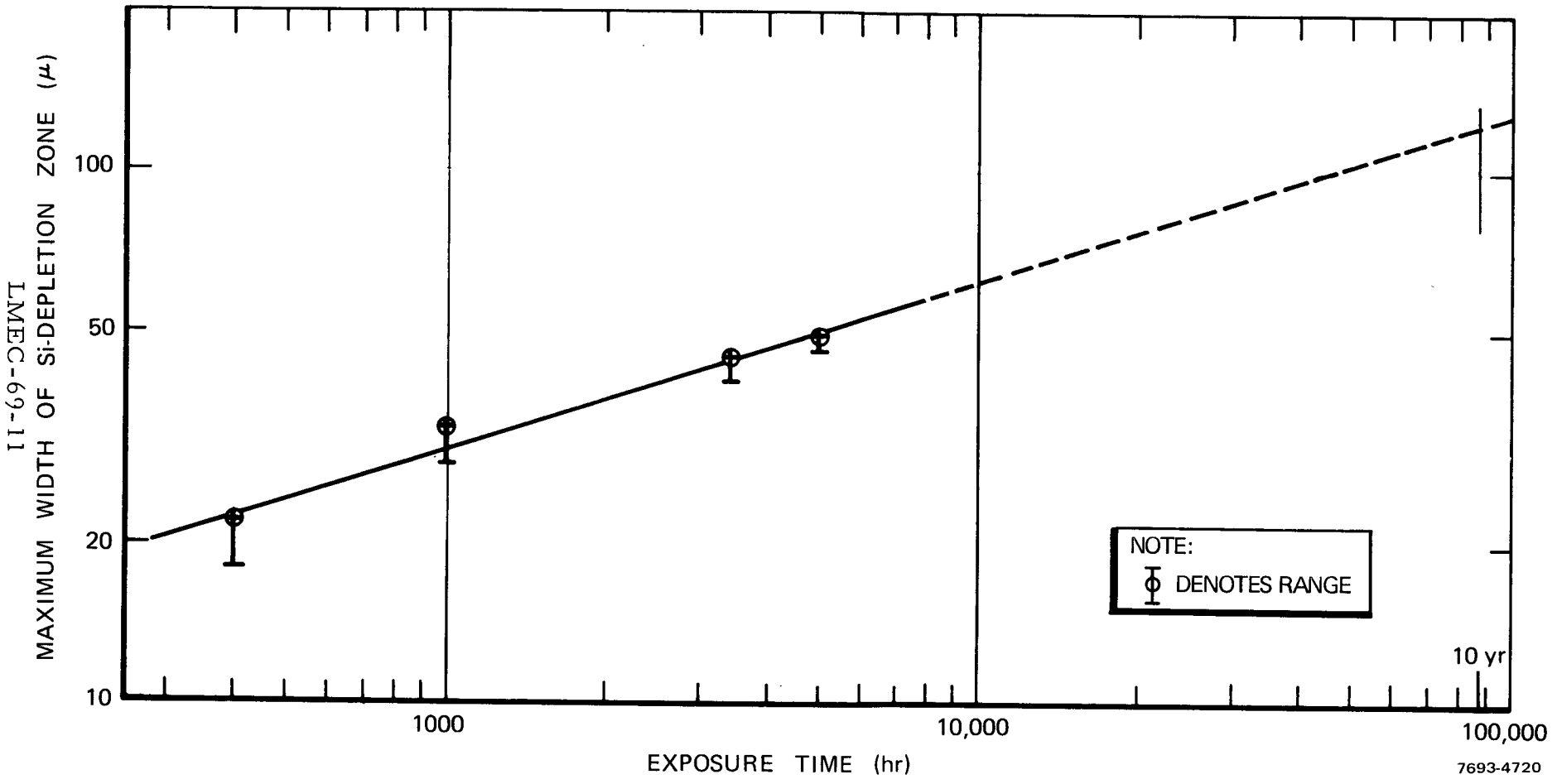

Figure 12. Silicon Depletion of Type 18-18-2 SS in 1200°F Sodium (O_2 ~30 ppm)

attributed to the dissolution of silicon in liquid sodium. This silicon depletion in a static liquid-sodium environment is further substantiated by the experimental data obtained by Agapova, et al., and by Jansen.[9,10] However, it is interesting to note that the oxidation rate constant for silicon is also logarithmic at high temperatures.[7] It appears, therefore, that the depletion rate could be controlled by the diffusion of silicon across the thin amorphous silica (oxide) layer.[7] This hypothesis suggests that the oxidation of silicon (reaction with the oxygen impurity in sodium), with the subsequent formation of a thin amorphous silica film, could contribute to the silicon depletion process. Further studies are required to thoroughly define this phenomenon.

Based on the extrapolated data in Figure 12, the rate of silicon depletion is acceptable – approximately 0.005 in. for 10 yr. However, the silicon depletion is reported to increase with oxygen concentration in sodium.[9] Therefore, the silicon depletion rate obtained in this experiment ($\sim$30 ppm O_2) would be high when compared to that expected in a normal LMFBR sodium environment (O_2 $\sim$15 ppm).

D. EFFECT OF SILICON DEPLETION

As shown in Figure 13, adding silicon to alloys produces a dual effect on the intergranular corrosion susceptibility of austenitic Fe-Cr-Ni alloys.[2] Characteristically, at low concentrations (0.3 to 1.5%), silicon acts to promote intergranular corrosion susceptibility, while at high concentrations, silicon acts to prevent such susceptibility. Based on corrosion tests in nitric acid, and electrochemical measurements in boiling nitric acid-dichromate solutions, Desestret[11] concluded that silicon accelerates the anodic dissolution of the grain boundaries but simultaneously forms a passivating film similar to that reported by Rhodin.[12] This film would act to inhibit the cathodic process and thus the anodic process, hence, reducing the entire corrosion process. Because of the dual effect of silicon on the intergranular corrosion resistance of Fe-Cr-Ni-Si alloys, the silicon depletion in Type 18-18-2 SS may have a significant deleterious effect on its stress-corrosion resistance. Consequently, actual stress-corrosion tests are highly warranted in order to quantitatively determine the effect of silicon depletion on the overall stress-corrosion resistance of Type 18-18-2 SS.

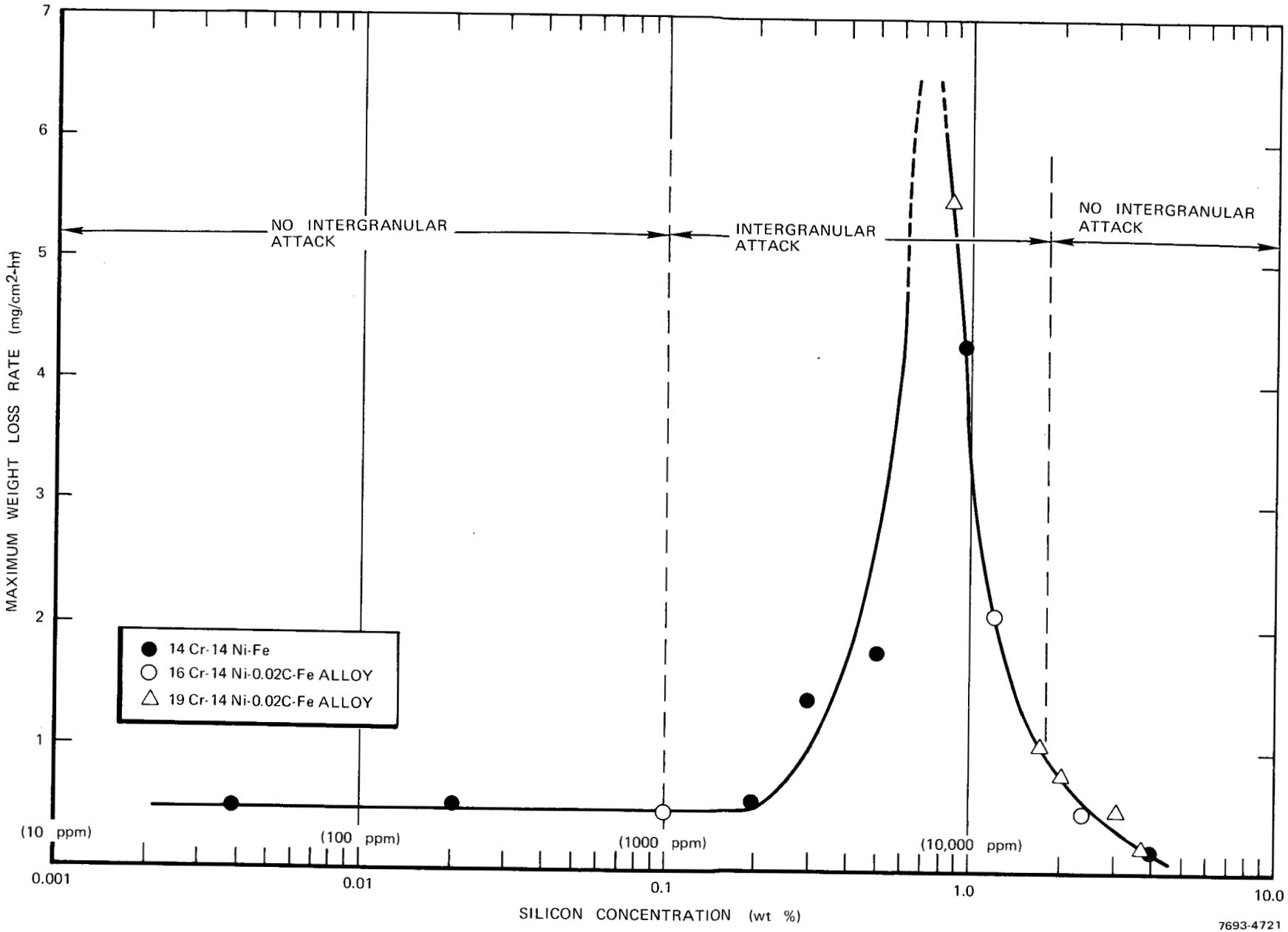

Figure 13. Effect of Silicon Additions on the Corrosion Resistance of 14 Cr - 14 Ni - Fe Alloys in $HNO_3 + Cr^{+6}$ Solution(2)

V. CONCLUSIONS

Initial corrosion studies of Type 18-18-2 SS in 1200°F static sodium (O_2 ~30 ppm) revealed the following:

1) Type 18-18-2 SS exhibited acceptable corrosion resistance in sodium even though it experienced a slightly higher corrosion rate than that of Type 304 SS.

2) The corrosion rate of Type 18-18-2 SS was logarithmic up to 3400 hr in sodium. But observable exfoliation of surface oxide ($NaCrO_2$) film occurred in samples exposed to sodium beyond 3400 hr.

3) Silicon depletion in Type 18-18-2 SS was of limited depth after 5060 hr in 1200°F sodium, and it increased logarithmically with time. In addition, chromium and manganese were depleted in the surface depletion zone. This surface compositional change resulted in the formation of a ferrite layer beneath the surface oxide film.

In summary, the exposure of Type 18-18-2 SS to 1200°F sodium produced two divergent observations relative to its performance in sodium. The indicated rate of silicon depletion and other compositional changes suggest that no detrimental changes would be anticipated over the time spans being considered for LMFBR applications. However, the indication of early breakaway of non-adherent surface films introduces a limitation that could disqualify Type 18-18-2 SS for sodium service.

VI. RECOMMENDATIONS

Based on the results of these corrosion tests, Type 18-18-2 SS shows sufficient promise to warrant further evaluation. It is recommended that additional testing, under controlled conditions, be performed:

1) To determine the long-term (beyond 5060 hr) corrosion behavior of the alloy in a liquid sodium environment. Since breakaway of a nonadherent surface oxide layer may accelerate corrosion by exposing new surfaces for attack, long-term tests will determine the effect of this nonprotective film on overall corrosion behavior in liquid sodium.

2) To study the corrosion behavior of Type 18-18-2 SS at other liquid sodium temperatures within the interest of the LMFBR Program. Such information would provide an understanding of the mechanism controlling the corrosion behavior of Type 18-18-2 SS and indicate temperature limitations, if any.

3) To determine the effect of sodium impurities (metallic and nonmetallic) on the corrosion resistance (including mass transfer) of Type 18-18-2 SS.

4) To assess corrosion product formation and adherence in a dynamic sodium system under simulated LMFBR thermal cycling conditions.

5) To conduct stress-corrosion experiments to determine the effect of silicon depletion on the stress-corrosion resistance of Type 18-18-2 SS.

REFERENCES

1. A. W. Loginow and J. F. Bates, "Influence of Alloying Elements on the Stress Corrosion Behavior of Austenitic Stainless Steels," Corrosion 25(1), 15 (January 1969)

2. J. S. Armijo, "Intergranular Corrosion of Nonsensitized Austenitic Stainless Steels," Corrosion 24(1), 24 (January 1968)

3. H. H. Uhlig, Corrosion and Corrosion Control (2nd printing, p 279; John Wiley and Sons Inc., New York, 1964)

4. ASTM Standards, Part 31, p 453 (May 1967)

5. H. H. Klepfer, D. L. Douglass, W. V. Cummings, M. B. Reynolds, and K. C. Antony, "Remarks Concerning Materials for Nuclear Superheat Fuel Cladding," GEAP-4060,2 (1962)

6. I. S. Gil'Dencorn and I. L. Rogel Berg, "Effect of Silicon Additions on the Oxidation of the Ni-Cr Alloy," Physics and Metals of Metallography, 18, 131 (1964)

7. O. Kubaschewski and B. E. Hopkins, Oxidation of Metals and Alloys (2nd Edition, pp 50, 131, 232; Butterworths, 1962)

8. W. T. Lee, "Biaxial Stress-Rupture Properties of Austenitic Stainless Steels in Static Sodium," AI-AEC-12694 (June 1968)

9. N. P. Agapova, A. G. Ioltukhovskiy, and V. V. Romaneyer, "Behavior of Stainless Steels in Sodium in the 600-900°C Temperature Range," SM-85/51 IAEA Symposium on Alkali Metal Coolants, Corrosion Studies, and System Operating Experience, Vienna, Austria, Nov. 29-Dec. 2, 1966 (p 21)

10. D. H. Jansen, "Depletion of Minor Constituents from Coast Metals No. 52 and No. 53 Brazing Alloys During Various Exposure," ORNL-58-10-86 (Oct. 1958)

11. A. Desestret, "Influence of Composition of Stainless Steel on Behavior in Transpassivity and Particularly on Secondary Passivity," Bull Circle Etudes Metaux 9(10), 365-435 (1965)

12. T. N. Rodin, "Oxide Films on Stainless Steels," Corrosion 12, 123t (1956)